SENSITIVITY OF PORE-SCALE DISPERSION TO PROPERTIES OF RANDOM BEADPACKS

ROBERT S. MAIER[1], MARK R. SCHURE[2], JUSTIN P. GAGE[3], JOSEPH L. SEYMOUR[3]

[1]U.S. Army Engineer Research and Development Center, Vicksburg, MS, [2] Rohm and Haas Chemical Co., Springhouse, PA, [3] Department of Chemical Engineering, Montana State University.

Abstract

Comparisons between pore-scale simulations and physical experiments are complicated by the difficulty of reproducing the geometry of the experimental porous medium. Flow and dispersion are affected by differences in packing density, random packing variation, packing defects, and confining walls. We quantify the sensitivity of pore-scale simulations to these parameters and compare dispersion behavior in packed columns between NMR experiments and pore-scale simulations. A conclusion is that the pore-scale simulations systematically underestimate dispersion in the experimental setting.

1. Introduction

Solute flow and dispersion in packed beds is fundamental to many industrial separation processes. Flow columns are also widely used for experimental investigations of transport in porous media. Hence, there is a need for accurate pore-scale simulation methods to aid in the design of new technologies and experimental techniques for measurement of transport properties. Pore-scale simulation is a relatively recent approach, and there are many sources of variation that complicate comparisons between simulation and experiment. Consequently, the ability to compute accurate simulation results at length and time scales corresponding to physical experiments is not yet clearly in hand.

In this paper, we consider the problem of comparing pore-scale simulation with NMR spectroscopy results on flow and dispersion in columns packed with monodisperse beads. We focus on the sources of variation arising from the representation of the beadpack. We do not explicitly consider numerical errors arising from the simulation, nor do we analyze the sources of experimental error. These are important factors that have been addressed elsewhere.

Given a monodisperse, random beadpack, we consider the effect of certain packing variations on the hydrodynamic dispersion coefficient obtained by pore-scale simulation. The sources of variation considered here include porosity, radial distribution function, bead size distribution, packing defects, and wall-induced ordering. Variations in the radial distribution function (RDF) of random packings imply more or less variation in nearest-neighbor distances. Although bead size distributions may be bidisperse or polydisperse,

Date: March 15, 2006.

we consider only the effect of mild monodispersity as compared to a monosize bead packing.

2. Overview of Pore-Scale Simulation Methods

In this section we provide a brief overview of our techniques for pore-scale simulation. For a more complete explanation, including the procedures for validation, the reader is referred to references [1, 2, 3].

2.1. **Packing Simulation.** Monodisperse spheres are randomly packed using a hard-sphere Monte Carlo algorithm. Spheres of uniform diameter, d, are arranged initially in a dilute cubic array. Each sphere is moved in a random direction and the move is accepted if it does not result in a collision with another sphere. After a series of such Monte Carlo steps, the minimum distance δ between sphere centers is evaluated and the coordinate system is scaled by the factor $d/[d + \Omega(\delta - d)]$ while maintaining constant sphere diameter, and where $0 < \Omega \leq 1$. By compressing the coordinate system, the packing density is increased. The rate of compression is regulated by Ω. For $\Omega = 1$ the packing is compressed as fast as possible without causing particle intersection. For $\Omega = 0$, the pack is not compressed. Thus, larger values of Ω correspond to more rapid compression. For packed cylinders, the array is contained within a cylinder with periodic boundaries at the ends. For an unconfined packing, periodic boundaries are used in all three dimensions. For packed cylinders, only the longitudinal coordinate is scaled, while for the unconfined packings, all three coordinates are scaled.

2.2. **Fluid Flow Simulation.** Fluid motion in the pores of a packed bed can be described by the incompressible Navier-Stokes equations

$$\rho \left[\frac{\partial \mathbf{v}}{\partial t} + (\mathbf{v} \cdot \nabla)\mathbf{v} \right] = \rho F - \nabla p + \mu \nabla^2 \mathbf{v} \tag{1}$$

with appropriate initial and boundary conditions, where $\mathbf{v}$ denotes the pore velocity, μ the dynamic viscosity, F a body force and p the pressure. We simulated three-dimensional viscous flow in the pore spaces of the packed beds with a lattice-Boltzmann (LB) method. The LB method solves the discrete-velocity Boltzmann equation using a finite difference discretization on a lattice of cubic cells [4]. In dimensionless form,

$$f_i(\mathbf{r} + \mathbf{e}_i, t + 1) = f_i(\mathbf{r}, t) - \frac{1}{\theta}\left[f_i(\mathbf{r}, t) + f_i^{EQ}(\rho, \mathbf{v}) \right] + F(\mathbf{r}) \cdot \mathbf{e}_i, \ i = 1, \ldots, q, \tag{2}$$

where the position vector $\mathbf{r}$ denotes the center of the cell, and f_i denotes the mass distribution function which propagates along the lattice velocity vector $\mathbf{e}_i$. These vectors and the equilibrium distribution function, f_i^{EQ}, are given by the d3q15 discretization. The local density and velocity are defined as the moments of the mass distribution functions, given in dimensionless form by

$$\rho = \sum_{i=1}^{q} f_i, \ \rho \mathbf{v} = \sum_{i=1}^{q} f_i \mathbf{e}_i \tag{3}$$

We set the relaxation parameter, θ, to unity for all simulations, to conserve memory and simplify the calculation. We use a constant body force F to model a uniform pressure gradient in the longitudinal (z) direction. The no-slip condition is enforced at solid surfaces using the bounceback technique and periodic boundary conditions are used elsewhere.

A solution with specified mean pore velocity is evolved from the initial condition, $\mathbf{v} = 0$ everywhere, by specifying a finite value of F and iterating the time-dependent LB equation. As the solution approaches steady state, the mean longitudinal velocity, $\bar{v}$, is evaluated and F is adjusted accordingly until the specified velocity is obtained within a small tolerance.

2.3. **Dispersion Simulation.** Transport was modeled by the motion of tracer particles governed by the Langevin equation. The Langevin equation for the position of an individual tracer was solved by the forward Euler method [6],

$$\mathbf{r}(t + \Delta t) = \mathbf{r}(t) + \mathbf{v}(\mathbf{r}(t))\Delta t + \xi\sqrt{2D_{\mathrm{m}}\Delta t} \tag{4}$$

where $\mathbf{r}$ is the position vector, $\mathbf{v}(\mathbf{r})$ is interpolated from the LB velocity field and ξ is a random vector on the surface of a sphere of radius $\sqrt{3}$. A modification of equation (4) is required to honor the no-flux boundary condition at solid surfaces. We use the approach in Salles et al.[7, 8], where particle trajectories are terminated at a solid boundary and the time step, Δt, is truncated in proportion to the step length. This results in a random angle of departure from the boundary in the subsequent time step, when a new random vector ξ is generated.

The time-dependent longitudinal dispersion coefficient is calculated from the tracer displacements as

$$D_L(t) = D_{zz}(t) = \frac{1}{2N}\frac{d\sigma^2}{dt} = \frac{1}{2N}\frac{d}{dt}\sum_{i=1}^{N}(\Delta z_i - \overline{\Delta z_i})^2 \tag{5}$$

where $\Delta z = z(t) - z(0)$ is the displacement at time t, and $\overline{\Delta z}$ is the ensemble average (and similarly for the transverse dispersion coefficient, $D_T = D_{xx} = D_{yy}$).

For all simulations we used a uniform initial concentration of one tracer per fluid lattice cell. In a packed cylinder, this corresponds to a solute slug of length L, where L is the length of the packed cylinder geometry. During the course of simulation, the solute slug is advected downstream (and spreads by diffusion) into the adjacent periodic image. However, as we have noted, the mean displacement is less than L.

3. Effect of Porosity, Nearest-Neighbor Distance, and Monodispersity on Dispersion

Variations in porosity evidently have only a weak effect on the hydrodynamic dispersion coefficent. D_L varies by little more than 10% over the range $.36 \leq \epsilon \leq .50$ (Figure 2). These results were obtained by gradually compressing a single packing to 50%, 45%, 40%, and finally to 36% porosity. We therefore assume the resulting four packs have similar local coordination and that we have controlled, to some extent, random variations in microstructure between the different porosities. It is interesting that D_L goes through a minimum around $\epsilon \approx 40\%$. What is perhaps more surprising, the 10% variation due to porosity is not much greater than "statistical" random packing variations at a single

porosity. Variations in D_L due to different random seeds were less than 7% for different beadpacks of the same porosity [1]. A tentative conclusion is that variations in D_L due to small porosity differences are of the same order as those induced by random packing variation.

The RDF, also denoted as $g(r)$ or $g_2(r)$, is calculated as a function of the nondimensional distance r/d where r is the dimensional distance and d is the packing particle diameter. The RDF $g(r)$ gives the probability of finding a pair of spheres a distance r apart, relative to the probability expected for a completely random distribution at the same density. The method of calculation is described in references [9, 10].

Figure 1 shows the RDF in four monosize beadpacks of the same porosity, differing in the speed of compression. Consider the first coordination shell in Figure 1 where $g(r/d) \approx 1$. The beadpacks compressed more quickly ($\omega = 0.9, 0.5$) have higher peaks near $g(r/d) = 1$, and have greater density where $g(r/d) > 1.2$. The interpretation is that slower compression allows the beads to distribute themselves more evenly, yielding a somewhat more uniform distribution of distance between neighbors.

Apparently small differences in the RDF lead to nearly a 30% difference in the hydrodynamic dispersion coeffcient. D_L/D_M ranges from 190 to 250 for different choices of the compression parameter, ω (Figure 2). Lower D_L correspond to the more slowly compressed packs. As a practical matter, we use slow compression ($\omega = 0.01$) in packing simulations, because packs are less likely to jam before reaching a desired packing density. Therefore, if experimental packings actually resemble the quickly-compressed beadpacks, our dispersion simulations may systematically underpredict experimental dispersion coefficients.

Mild monodispersity does not appear to have much effect on the dispersion coefficient. Beads were drawn from the uniform distribution of radii, $r \in U[.45, .55]$, and a set of beadpacks were obtained as described above, by compressing to progressively lower porosities. The resulting monodisperse beadpacks differ little from the monosize beadpacks of the same porosity in their dispersion coefficients (Figure 2). This result suggests variations in D_L due to mild monodispersity are also of the same order as those induced by random packing variation.

4. Effect of Packing Defects on Dispersion

As part of an earlier investigation by Schure [11], a number of "defective" beadpacks were created by selectively removing particles in clusters or in lines from an undisturbed pack with $\epsilon = .36$. Here we have selected a subset of the defective beadpacks and obtained solute dispersion coefficients, to understand the potential magnitude of variations induced by packing defects. Figure 3 shows particle removal sites for the five beadpacks. The defects created by particle removal are quite large and not necessarily representative of an experimental packing. Thus, it is especially surprising that the resulting flow and dispersion behavior in one of these beadpacks (the least defective) is similar to a non-defective beadpack.

Figure 4 shows the time-dependent dispersion coeffcients obtained from the defective beadpacks. In beadpack D1, the dispersion coefficient is comparable to the non-defective packs (see Figure 2) of same porosity. The interpretation is the defects in D1 are isolated and relatively small and do not introduce any new length scale to the medium.

The situation is quite different for larger defects, and it is interesting to observe the dispersion coefficients in beadpacks D6, D7, and D12 remain preasymptotic. These beadpacks have line defects that provide a fast flow path. The line defect introduces a new length scale, proportional to the column width. Solute particles must trasverse the column and find the preferential flow path in order to contribute, in a statistical sense, to the dispersion coefficient.

5. Effect of Confining Walls on Dispersion

Schure's investigation [11] of defective beadpacks shows that a preferential flow path may introduce a new length scale for solute dispersion. The situation in a packed cylinder is analogous because the packing effects induced by the confining wall create regions of faster flow. Figure 5 shows the normalized velocity distribution in a cylindrical beadpack, averaged in the radial direction. Note the amplitude of the flow variation is quite similar in cylinders ranging in diameter from $10d$ to $50d$.

In the case of a cylindrical beadpack, the relevent time scale for dispersion is proportional to R^2/D_T, the time required for tracers to disperse laterally in the column, where R is the cylinder radius and D_T a transverse dispersion coefficient [2]. This time scale is generally quite long compared to experimental time scales, especially NMR experiments. However, the effect of confining walls on the time-dependent dispersion coeffcient is already manifested at very short times. This was observed in simulation by comparing the time-dependent behavior of $D_L(t)$ in confined cylindrical beadpacks with unconfined (periodic) beadpacks and cylindrical beadpacks without wall-induced ordering (i.e., by superimposing a confining cylinder on an originally-unconfined beadpack). Figure 6 shows the relative magnitude of dispersion coefficients in these different beadpacks. Note $D_L(t)$ is up to 30% higher in the cylinders than in the unconfined beadpack.

Although interesting, this result does not necessarily complicate comparisons between simulation and NMR experiments, as long as a cylindrical beadpack of similar diameter is used in simulation. On the other hand, the result presents a real complication if comparisons are made between simulations and experiments on different time scales. Breakthrough experiments are typically conducted on an intermediate time scale that, while shorter than R^2/D_T, is much longer than typical simulation time scales. In such a comparison, the experimental dispersion coefficient will be significantly greater than one obtained at shorter times.

6. Comparison with NMR PGSE Results

There are strong analogies between NMR experiments and pore-scale simulations of hydrodynamic dispersion. NMR pulsed gradient spin echo (PGSE) experiments measure a signal emitted from a selected portion of a flowing column that corresponds to the displacement of water molecules initially marked with a distinguishable magnetic spin [12]. The PGSE experiment is, in effect, a tracer study that dynamically captures the distribution of molecular displacements. Pore-scale simulations often use a stochastic Langevin equation to simulate the motion of Brownian particles in a pore-scale fluid flow field. A large number of such particles are tracked through the pore spaces and they also provide a dynamic distribution of particle displacements, and hence, a time-dependent dispersion coefficient. NMR PGSE experiments are limited in duration to a time proportional to

the attenuation of a magnetically-induced molecular spin orientation. This time scale is relatively short compared to conventional column breakthrough experiments. Pore-scale simulations are also limited to a similar time scale, because of the need to represent a sufficiently large section of the column at an appropriate level of numerical resolution. Given these analogies, it is possible to conduct NMR PGSE experiments and pore-scaled simulations on similar physical domains and time scales. The major difference is in the realization of the beadpack geometry.

Gage and Seymour [13] have studied dispersion in packed columns using PGSE techniques. They apply a Fourier transformation to the echo attenuation function, yielding the density function of molecular spin displacements, also known as the *propagator* function, given by $P(z, \Delta)$, where z is the displacement along the axial direction and Δ the displacement time. Figure 7 shows the propagator function obtained at three different displacement times from one column. In Figure 7(a), the displacement time is small; a tracer traveling at the mean velocity has traveled only 0.4 bead diameters. The propagator function has an exponential shape similar to the underlying velocity density function. In Figure 7(b), a tracer traveling at the mean velocity has traveled 2 bead diameters. Note there are three peaks in the propagator. The rightmost peak is most closely associated with the center of mass. The interpretation is that fluid initially moves around a bead and then may either be diverted laterally, slowing displacement along the z-axis, or may continue downstream. The diverted fluid forms the residual peak. The process is repeated for another bead diameter, and a second residual peak is formed, while the earlier peak has dissipated. Within a few bead diameters, most tracers have sampled the lateral motion, and the residuals have disappeared. In Figure 7(c), a tracer traveling at the mean velocity has traveled 6 bead diameters, and the propagator functions appear Gaussian. The interpretation is the dispersion coefficient roughly approximates the core region of the column. However, if the measurement is continued, the coefficient will continue to grow as more tracers sample the flow heterogeneities near the wall.

We developed pore-scale simulations corresponding to the Gage and Seymour experiments and have compared the propagator functions from simulation and experiment in Figure 7. In Figure 7(a), the simulation propagator is slightly more dispersed than the NMR propagator, but they are qualitatively similar. In Figure 7(b), the simulation propagator is less dispersed than the NMR propagator, and it's residual peaks are not visible in the plot. (A magnification of the simulation propagator reveals asymmetries in the trailing edge of the propagator that correspond to the residual peaks in the NMR propagator.) In Figure 7(c), the simulation propagator is less dispersed than the NMR propagator, but is qualitatively similar. (Note the simulation propagator corresponds to a dimensionless displacement time $\tau = 5$, while the NMR propagator corresponds to $\tau = 6$. Even accounting for this difference, the NMR propagator is significantly more dispersed.) After a displacement time of $\tau = 10$, the NMR dispersion coefficent is $D_L(t) = 1.2 \times 10^{-7}$, compared with $D_L(t) = 0.7 \times 10^{-7}$ in the simulation. Similar results are also found at a higher Peclet number. Thus, the simulations systematically underpredict the experimental dispersion coefficients.

7. Conclusion

Our pore-scale simulations underpredict hydrodynamic dispersion in NMR PGSE experiments. The underprediction is greater than the error associated with variations in porosity or bead size distribution. Major defects in the experimental beadpacks are also ruled out as an explanation. From a simulation viewpoint, there are at least two approaches for investigation. One is to search for systematic errors in the numerical simulation methods. A second approach is to identify beadpack characteristics associated with higher dispersion and try to correlate these characteristics with experimental beadpacks.

With respect to the numerical methods, we rely on the analytical solution for Taylor dispersion for validation. However, as there is no analytical solution to validate simulation results in a beadpack, the methods may have a systematic bias in that setting. One area of investigation involves the solution of the stochastic Langevin equation at complicated solid boundaries e.g., bead surfaces. The mathematical treatment of stopped diffusions is less developed than for unrestricted diffusion, and the effect of errors in solving these equations at boundaries is not really understood for the simulations of interest here.

To resolve the difference between NMR and simulation results, we take the presence of residual peaks in the short-time NMR propagators as an important clue, because these features do not appear in simulations. We do not yet know how to produce such peaks in the simulations. As noted above, the nearest-neighbor distance distribution has an influence on dispersion. Indeed, beadpacks that are compressed more quickly are more dispersive and, as the parameter ω is increased, the short-time propagators begin to develop weak bimodality. The D5 'defective" beadpack, which is characterized by cluster defects and is very dispersive, also has a propagator with a weakly bimodal distribution at short times. We intend to continue this line of investigation by examining the effect of other modifications to beadpack microstructure.

References

[1] R. S. Maier, D. M. Kroll, R. S. Bernard, S. E. Howington, J. F. Peters, and H. T. Davis, Pore-scale simulation of dispersion, *Phys. Fluids* **12**, 2065 (2000).

[2] R. S. Maier, D. M. Kroll, R. S. Bernard, S. E. Howington, J. F. Peters, and H. T. Davis, Hydrodynamic dispersion in confined packed beds, *Phys. Fluids* **15** (12), 3795 (2003).

[3] R. S. Maier, D. M. Kroll, H. T. Davis, and R. S. Bernard, Pore-scale flow and dispersion, *International Journal of Modern Physics C* **9** (8) 1523 (1998).

[4] J. D. Sterling and S. Chen, Stability analysis of lattice Boltzmann methods, *J Comp Phys*, **123**, 196 (1996).

[5] H. Chen, S. Chen, W. H. Matthaeus, Recovery of the Navier Stokes equations using a lattice-gas Boltzmann method, *Physical Review A*, **45** (8), R5339-R5342 (1992).

[6] P. E. Kloeden and E. Platen, *Numerical Solution of Stochastic Differential Equations,* Applications of Mathematics Series Vol. 23, Springer-Verlag, Heidelberg (1992).

[7] J. Salles, J.-F. Thovert, R. Delannay, L. Prevors, J.-L. Auriault, and P.M. Adler, Taylor dispersion in porous media. Determination of the dispersion tensor, *Phys. Fluids,* **5** (10), 2348 (1993).

[8] J.J. Tessier, K.J. Packer, J.-F.Thovert, and P.M. Adler, NMR measurements and numerical simulation of fluid transport in porous solids, *AIChE Journal,* **43** (7), 1653-1661 (1997).

[9] M. P. Allen, D. J. Tildesley, Computer Simulation of Liquids. Oxford Science Publications, New York, 1987.

[10] D. Frenkel, B. Smit, Understanding Molecular Simulation. Academic Press: San Diego, CA, 1996.

[11] M. R. Schure and R. S. Maier, How does column packing microstructure affect column efficiency in liquid chromatography?, *Journal of Chromatography A*, submitted.

[12] J.D. Seymour and P.T. Callaghan, Generalized approach to NMR analysis of flow and dispersion in porous media, *AIChE Journal,* **43** (8) 2096 (1997).

[13] J. P. Gage, *Magnetic Resonance Imaging of Time-Dependent Dispersive Transport Processes in Porous Media*, Ph.D. Thesis, Montana State University, 2006.

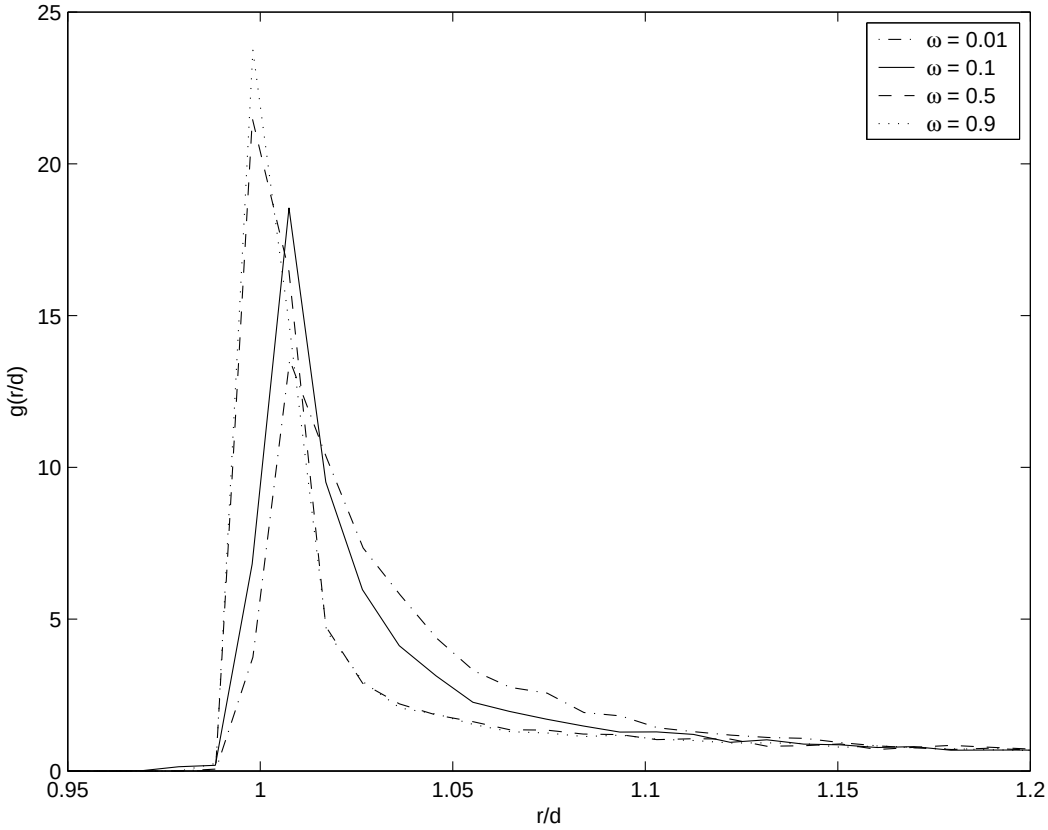

FIGURE 1. Radial distribution function near first coordination shell in four periodic beadpacks of dimensions $10d \times 10d \times 40d$ with $\epsilon = .40$. The parameter ω is related to the speed of compression during packing.

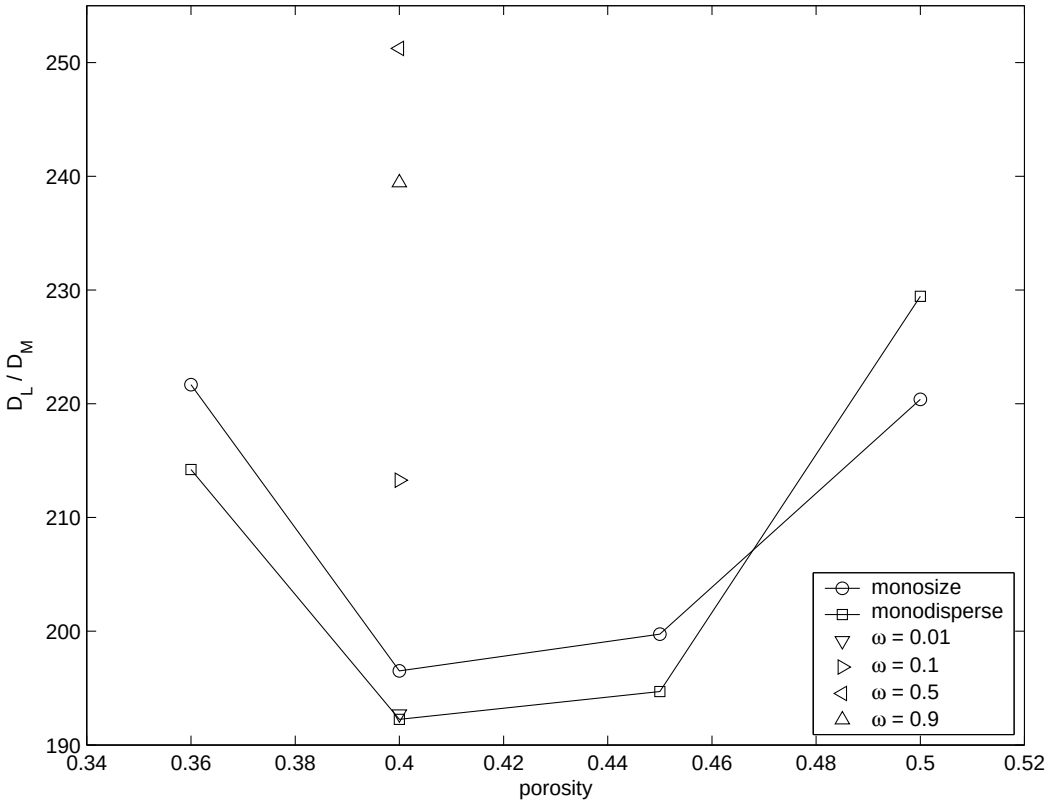

FIGURE 2. Longitudinal dispersion coefficients in periodic beadpacks of dimensions $10d \times 10d \times 40d$. The coefficients are asymptotic and correspond to an elapsed time of $\bar{v}t/d = 10$. $Pe = 476$ ($Re = 1$)

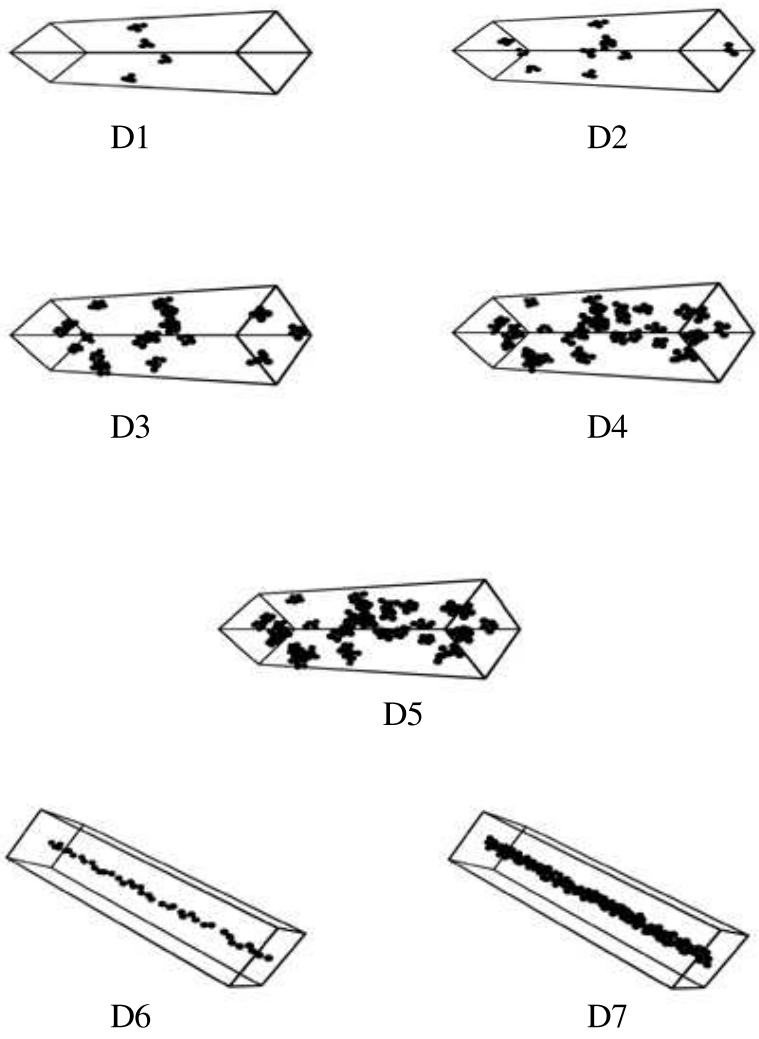

FIGURE 3. The seven defect packs used in the study labeled D1 through D7 where the spheres shown are the vacant defect sites in the pack. The periodic boundary box edges are highlighted.

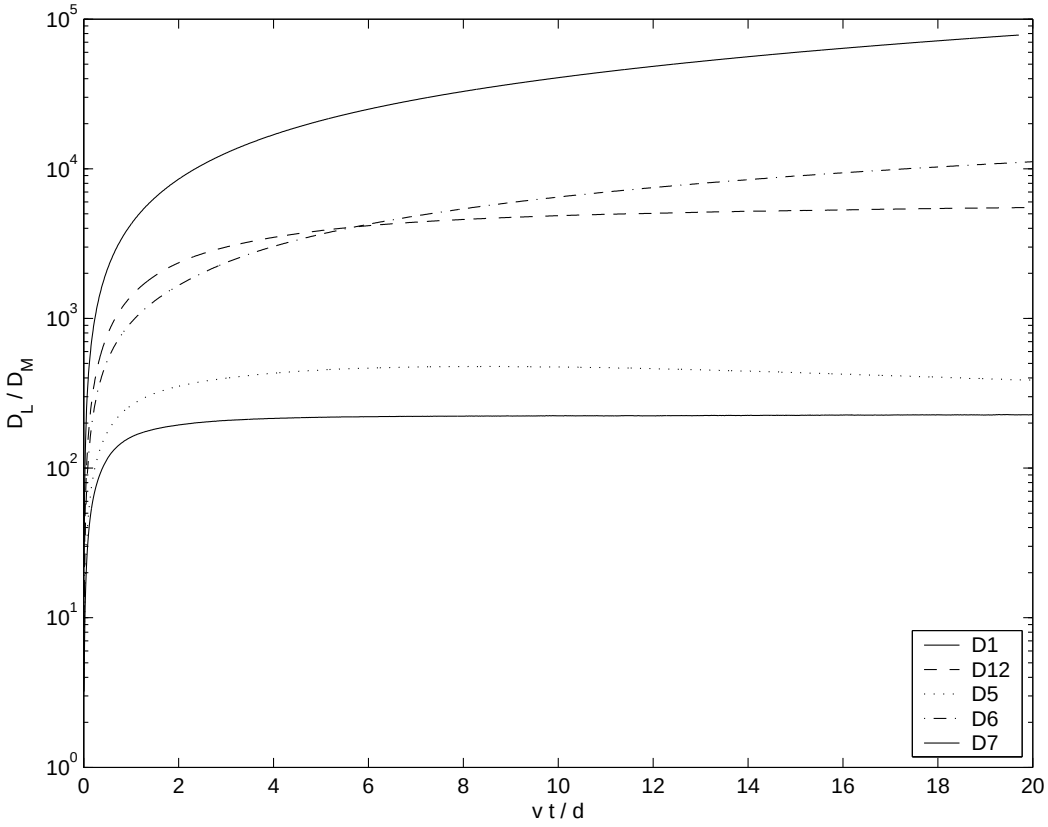

FIGURE 4. Time-dependent longitudinal dispersion coefficients in defective periodic beadpacks of dimensions $10d \times 10d \times 40d$. $Pe = 476$ ($Re = 1$)

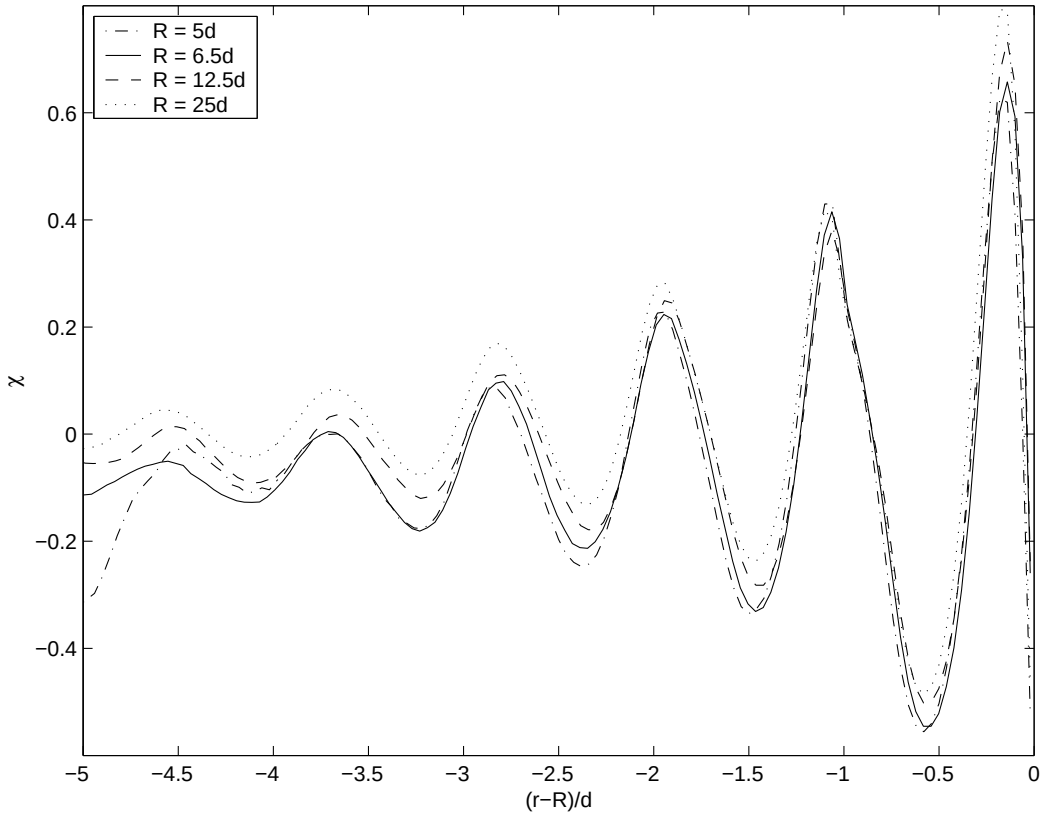

FIGURE 5. Average axial velocity (normalized) versus radial distance from the cylinder wall in four cylindrical beadpacks of different radius. The central region of the largest three columns is not shown. ($Re = 1$)

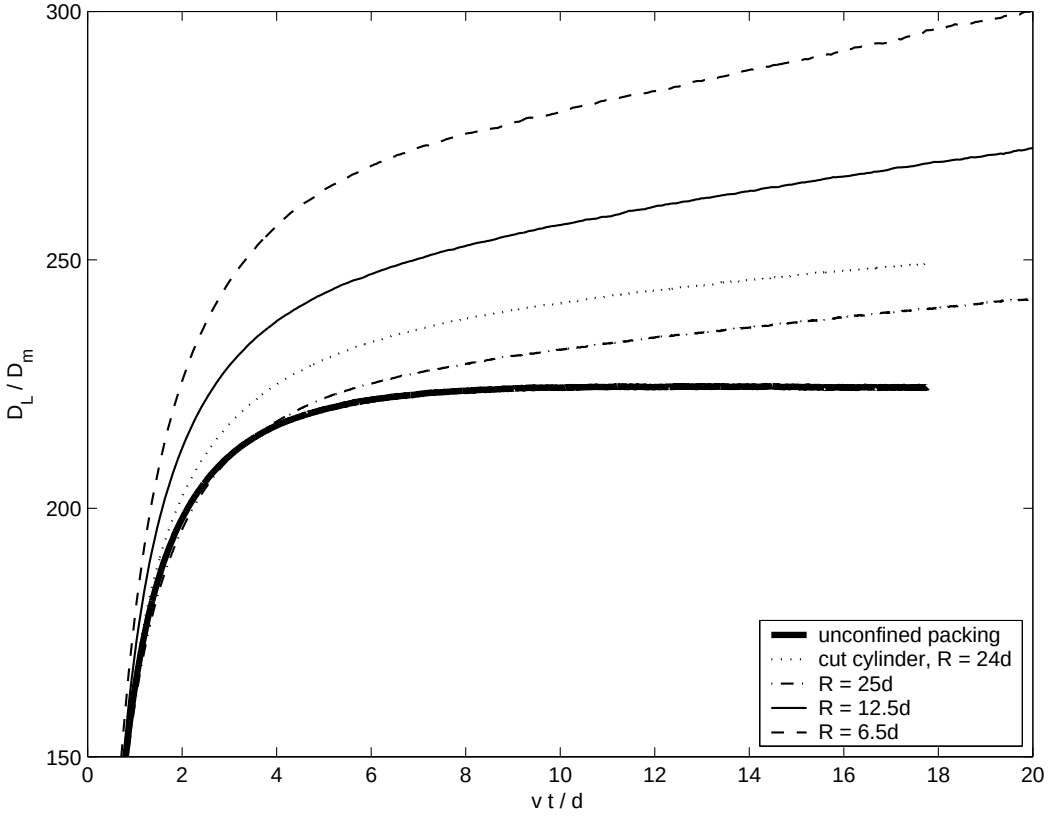

FIGURE 6. Time-dependent longitudinal dispersion coefficients in four cylindrical beadpacks of different radius and one periodic (unconfined) packing. The cut cylinder was created by superimposing a cylinder wall on the periodic packing. $Pe = 476$ ($Re = 1$)

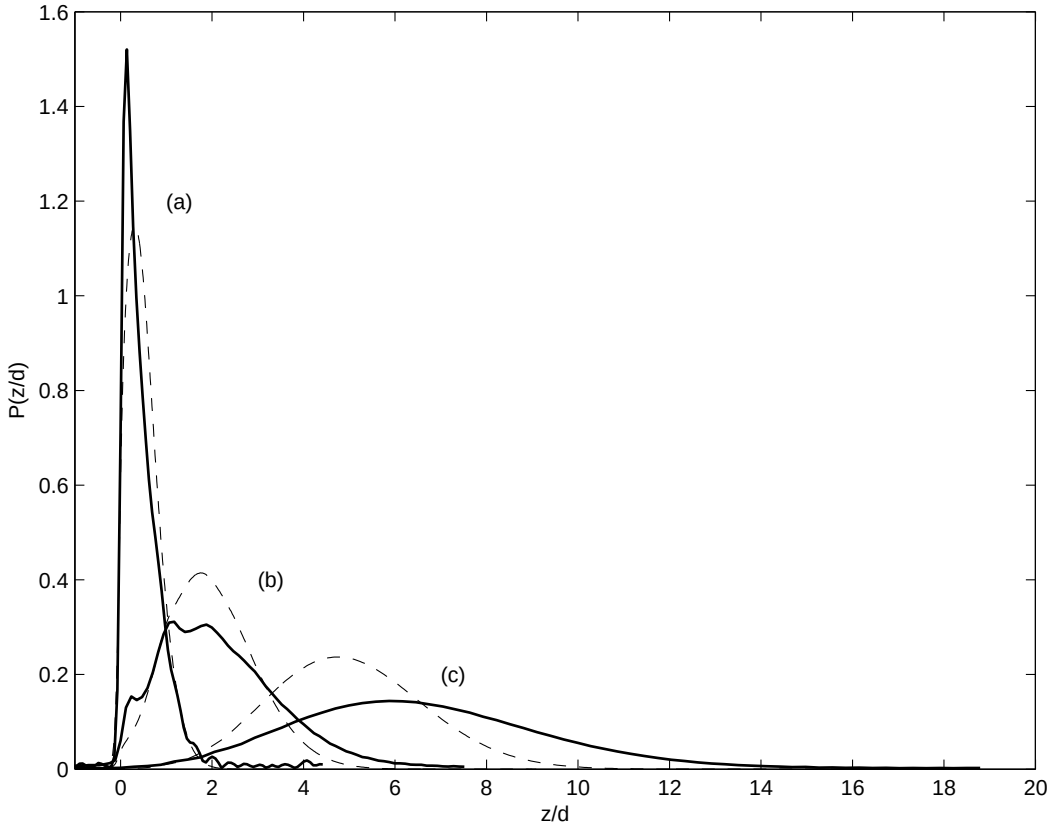

FIGURE 7. NMR propagators (solid line) and simulation propagators (dashed line) in a cylindrical beadpack of diameter $25d$, at three different times. Dimensionless times are given by $\tau = \bar{v}t/d$ and do not match exactly between simulation and experiment. (a) $\tau_{NMR} = 0.4$, $\tau_{sim} = 0.5$, (b) $\tau_{NMR} = \tau_{sim} = 2.0$, (c) $\tau_{NMR} = 6.0$, $\tau_{sim} = 5.0$. $Pe = 63$ ($Re = 0.2$) and $d = 100\mu m$